



Fragmentation of Mansurov granite under quasi-static compression

Marina Davydova, Ivan Panteleev, Oleg Naimark

Institute of Continuous Media Mechanics Ural Branch Russian Academy of Sciences

1, Ac. Korolev str., Perm 614013, Russia. <http://lab13.icmm.ru/index.php/en/>

1957davydova@gmail.com, pia@icmm.ru, naimark@icmm.ru



ABSTRACT. The fragmentation statistics was studied in the quasi-static compression experiments conducted on prismatic specimens of Mansurov granite. The statistical analysis showed that the cumulative fragment mass distribution for granite specimens is well described by a power law function, but the fragment number-sieve size distribution deviates from the power law in the range of are equal to about 1 mm. In order to explain this fact, we investigated the structure of fractured material (Computed Tomography and microstructures study in thin sections). A sharp increase the number of grains in the range of size from 0.5 mm to 1 mm and a change in the fragment shape (from splinter to oval) allow us to suppose that there is an addition fracture mechanism associated with disintegration of feldspar and amphiboles grains.

KEYWORDS. Fragmentation statistics; Granite fracture; Power law distribution.

Citation: Davydova, M., Panteleev, I., Naimark, O., Fragmentation of Mansurov granite under quasi-static compression, *Frattura ed Integrità Strutturale*, 42 (2017) 170-180.

Received: 25.06.2016

Accepted: 12.08.2017

Published: 01.10.2017

Copyright: © 2017 This is an open access article under the terms of the CC-BY 4.0, which permits unrestricted use, distribution, and reproduction in any medium, provided the original author and source are credited.

INTRODUCTION

Fragmentation plays an important role in a variety of geological phenomena, which is the main is due to the fact that rock fragmentation involves the initiation and propagation of fracture, and interaction between defects (pores, cracks) over a wide range of scales [1]. There exist many works devoted to different types and aspects of rock fragmentation. This phenomenon has been discussed by Grady [2,3]. Bowman [4] used the concepts introduced by Grady to study the dynamic fragmentation of rock during rock avalanches. Apart from the studies of natural process, there are many investigations on rock fracture under dynamic and quasi-static loading in laboratory conditions. A variety of methods and techniques are used to gain a complete understanding of the fracture mechanisms in rock: acoustic emission [5,6], fractolumiscence [7-9], digital image correlation [6,10], image analysis [11], electromagnetic emission [9,12-15] and nuclear emission [16,17]. In this work, along with the definition of fragmentation statistics laws, we study the granite structure of fragmented sample by using: X-ray Computed Tomography (CT), petrography-analysis of rocks in thin section, granulometric analysis and imaging particle analysis.

EXPERIMENTAL CAMPAIGN

The fragmentation statistics was studied in the quasi-static compression experiments, performed on prismatic specimens of Mansurov granite, with lateral dimensions of 50×50 mm and height of 100 mm. Ten samples were tested on the electro-mechanical testing machine Zwick/Roel Z250 having a capacity of 250 kN (in uniaxial compression tests). Grip displacement rate was controlled taken ranging between $0.02 \div 0.2$ mm/min. The experiments were performed at room temperature. The characteristic stress-strain curve for tested samples is given in Fig.1.

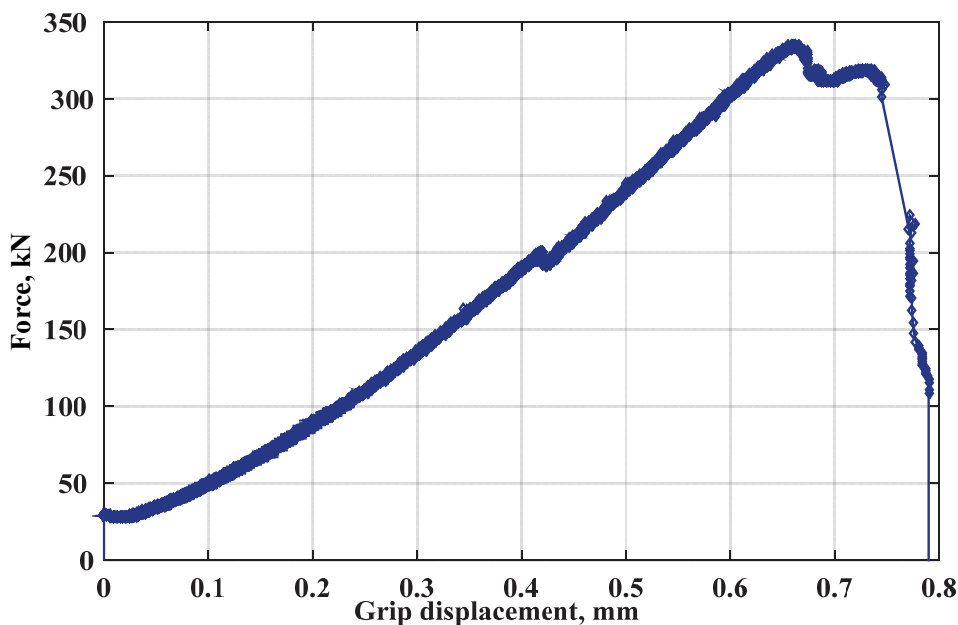


Figure 1: Characteristic stress-strain curve for granite specimens.

FRAGMENTATION STATISTICS

The study of fragmentation statistics generally involves the construction of the cumulative function of the fragment size distribution, i.e., determination of the relationships between the number of fragments N , the mass of which is larger than a prescribed value, and the mass m of the fragment. The fragment mass was measured by weighing each fragment on the electronic balance HR-202i (accuracy of the balance was 10^{-4} g). The large size fragments were weighed separately and small-size fragments were passed through a set of sieves, whose cell size varied from 0.315 to 15 mm. The number of fragments retained on sieves, N_s , was varied from 1 to 1.5×10^4 , (Fig.2(b)), and mean fragment mass for different sieves was varied from 4.5×10^{-5} to 3 g Fig. 2(a).

For the sieves with a great number of fragments, the procedure of determination of fragment number, N_s , consists of two steps: 1) definition of mean fragment mass, m_m ; 2) calculation of number, N_s , as:

$$N_s = M / m_m \quad (1)$$

where M is the total mass of fragments in the sieve. To calculate mean fragment mass, m_m , we weight 200 or 300 fragments. The mass of these fragments has to be greater than low balance limit 0.02 g. Fig. 2(b) presents a log-log plot of the cumulative fragment mass distribution for the ten granite samples. This distribution is well described (being $R^2 > 0.95$ for six samples, and $R^2 > 0.99$ for four samples) by the power law function:

$$N \cong Cm^{-D} \quad (2)$$

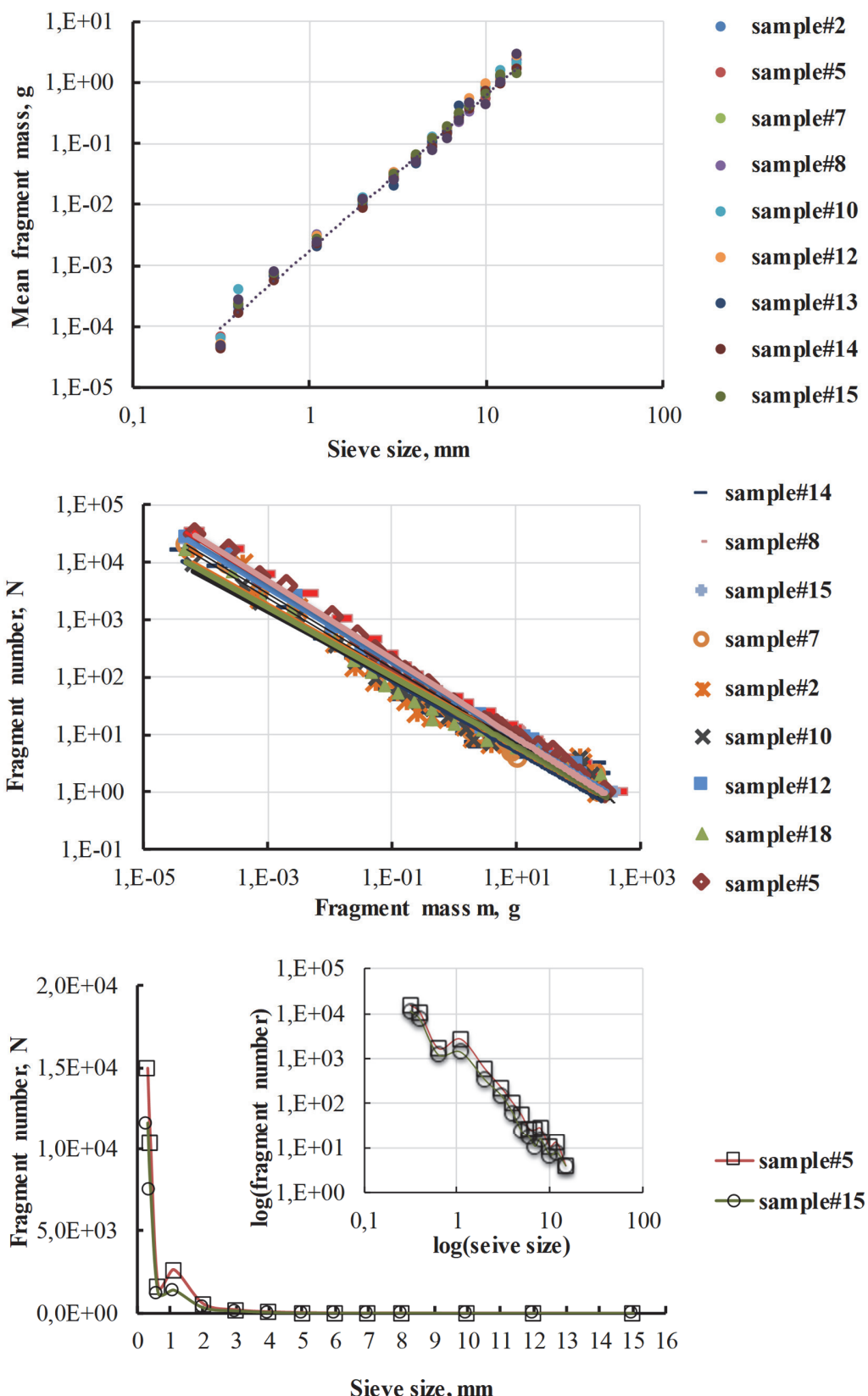


Figure 2: Statistics of fragmentation: a) mean fragment mass vs sieve size; b) cumulative fragment mass distribution; c) fragment number - sieve size distribution.

where the fractal dimension D varies in the range from 0.563 to 0.682, and C varies in the range from 25 to 42. The expression (2) is called the fractal number relation [1]. To evaluate the scatter of D , we tested at a grip displacement rate $V = 0.05$ mm/min four samples and at a value $V = 0.02$ mm/min three samples (Fig. 3). The coefficient of variation is 4% and 9% for grip displacement rate $V = 0.05$ mm/min and for $V = 0.02$ mm/min, respectively. It is evident that for a reliable conclusion would require extensive statistical sampling, but under the given loading condition we assume that the variation in D is caused by the material inhomogeneity. Moreover, in Fig. 3 it can be observed that the power law exponent D does not practically change when the grip displacement rate increases by a factor of ten. The fragment number-sieve size distribution has the feature in the range of about 1mm, Fig.2(c). Insert in Fig.2(c) illustrates this distribution in a log-log plot. If the fragment number-sieve size distribution is described by power law (in this case, the graph in insert of Fig.2(c) would be a straight line) the fragment number in the sieve with a cell size 1.1 mm will be lower than that obtained in experiments. This feature of fragment number-sieve size distribution is more or less pronounced, depending on the sample.

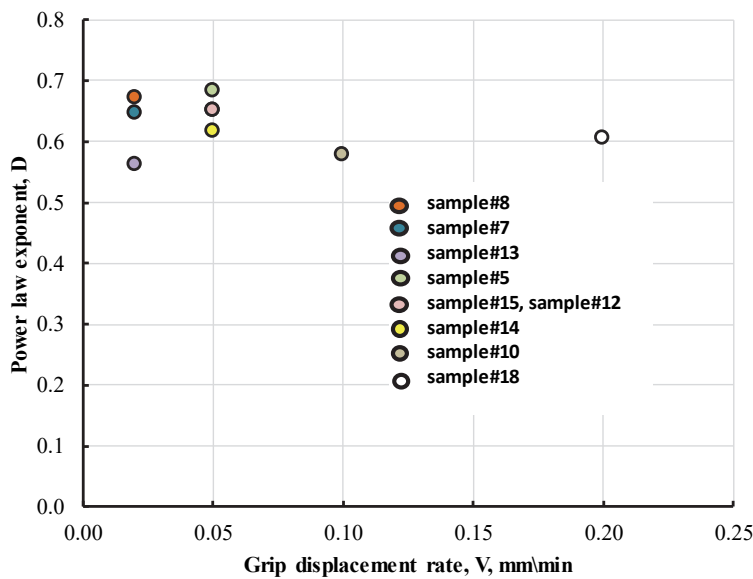


Figure 3: Power law exponent D vs grip displacement rate.

STRUCTURE STUDY

In order to understand the nature of this feature, the granite structure of fragmented sample was examined by using: X-ray Computed Tomography (CT), petrography-analysis of rocks in thin section, granulometric analysis and imaging particle analysis.

X-ray Computed Tomography (CT)

CT was performed for one of a big fragment with size, of about 28mm \times 9mm \times 9mm and mass 2.26g. This fragment has a big cluster of cracks, which illustrates the process of granite fragmentation (Figs.4). Blue color in the volume rendered CT image of this fragment indicates the crack cluster. Gray scale 2D image (Fig. 4c) allows us to conclude that Mansurov granite fracture can be both of transgranular as well intergranular character [7]. Using CT it is impossible to evaluate, which grains (plagioclase, potash feldspar or quartz) are responsible of fracture, because the density for these three minerals is practically the same (plagioclase density is 2620-2760 kg/m³; potash feldspar density is 2540-2750 kg/m³; quartz density is about 2650 kg/m³).

Petrography-analysis of rocks in thin section

Petrography-analysis was done using Polarizing microscope OLIMPUS BX51. It showed (Fig.5) that Mansurov granite has hypidiomorphic (with different degrees of idiomorphism of the grains of plagioclase, potash feldspar, quartz and hornblende) and porphyritic structure which the main part consists of plagioclase phenocryst. Texture of the rock is homogeneous and disorderly. Main rock-forming minerals are plagioclase (25-30%), potassium feldspar (25-27%), quartz (25-30%) and amphiboles (10%). Amphiboles are represented by hornblende and clusters of aggregates of actinolite needles.

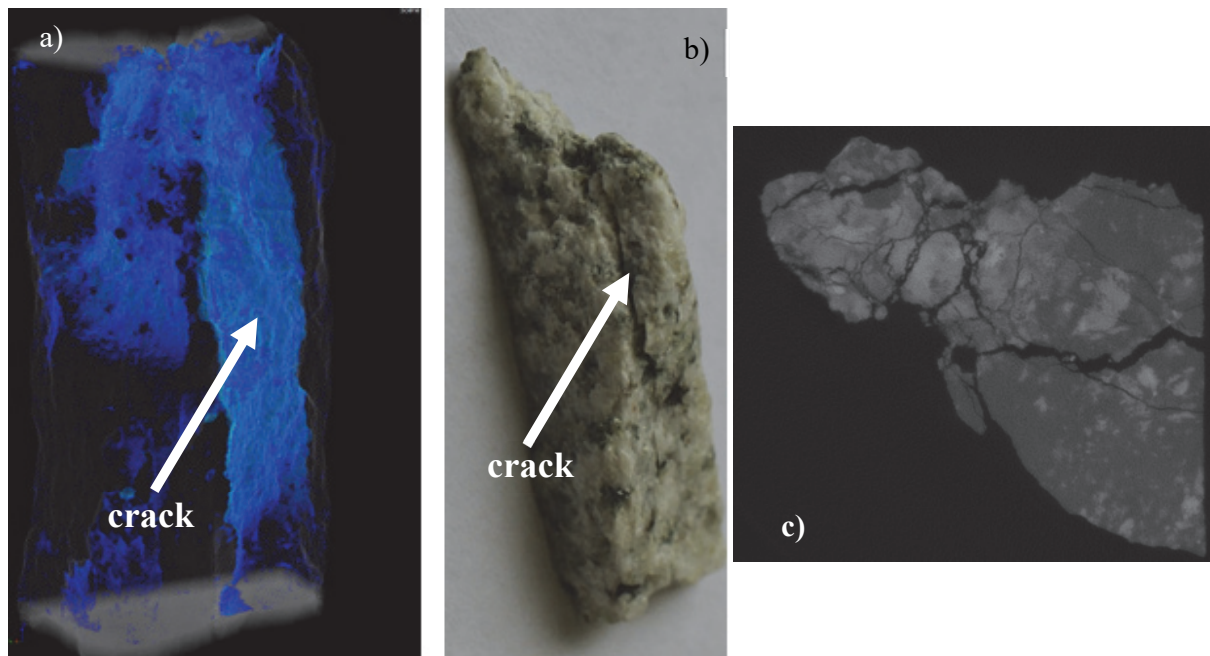


Figure 4: a) 3D X-ray Computed Tomography of the fragment (sizes $\sim 28\text{mm} \times 9\text{mm} \times 9\text{mm}$ and mass 2.26g); b) photo of the fragment; c) 2D Computed Tomography of the upper part of the fragment.

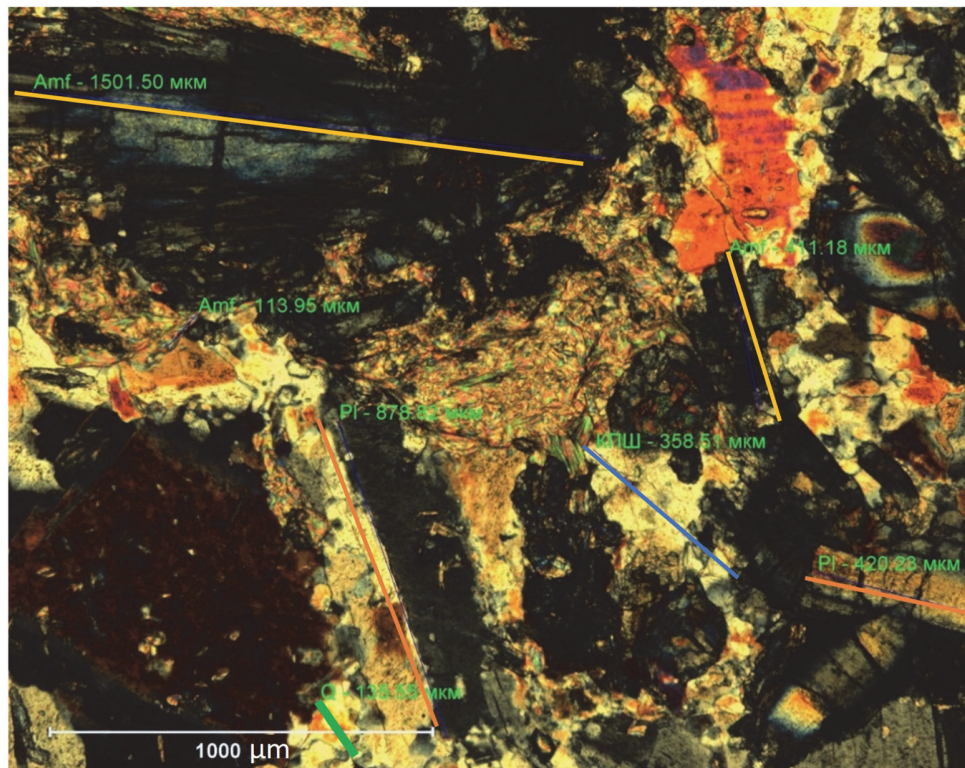


Figure 5: Petrography-analysis. A plagioclase grain is indicated by a red line, a potassium feldspar - by a blue line, a quartz - by a green line, and a amphiboles - by a yellow line (cross-polarized light, magnification $\times 50$).

The grain size analysis gives us the mean grain size. It was measured ten field of vision with total number of grain being 167. Most plagioclase grains have the size of about 0.25-0.5 mm; potassium feldspar – 0.5-1.0 mm; quartz and amphiboles

-0.1-0.25 mm. By analyzing the grain size– grain number distribution shown in Fig. 6 it can be seen that in the range 0.5÷1 mm number of grains increases more than five times. Most of the grains (60%) are Feldspar (Potassium feldspar and Plagioclase) and 40% are Amphiboles. For fragments with the size of more than 2 mm, the fracture mechanism is due to cracking (Fig. 4), whereas the formation of fragments of about 1mm can involve an additional mechanism of fracture, which is provided by chipping of feldspar and amphiboles grains. A considerable increase in the fragments number with the size less than 0.5 mm (Fig. 2(c)) may be caused by chipping of Quartz.

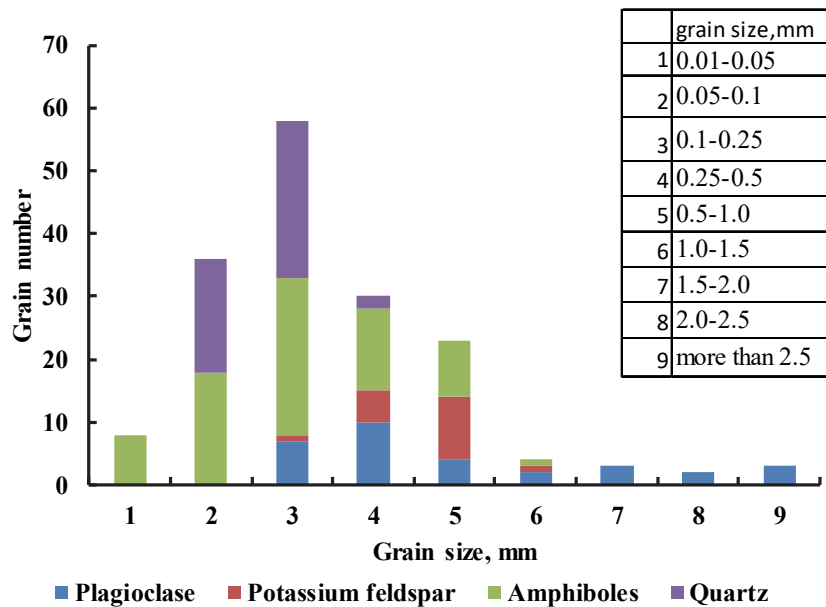


Figure 6: Statistical data on grain size.

IMAGING PARTICLE ANALYSIS

The imaging particle analysis was performed based on the photos of fragments collected in the sieves. The fragment shape is characterized by circularity, C , given by:

$$C = 4\pi \times S / P^2 \quad (3)$$

where S is the area and P is the perimeter of the fragment image in the photographs given in Fig.7. The circularity value equal to 1.0 indicates a perfect circle. A decrease in the sieve size leads to a growth of the circularity to 0.8 and narrowing of the scatter, Fig.8. This can be indicative of the fact that fragmentation on the small scale is defined by the structure of material and mainly by feldspar and amphiboles, the grain size of which is about 1mm. An increase of the circularity for the sieve with the cell size of 0.63mm, compared to the cell size of 1mm, is different for different samples, Fig. 9. It depends on the material structure of the samples.

COMPARISON WITH OTHER MATERIAL

We have analyzed fragmentation of six materials under five different loading conditions: i) granite fragmentation under quasi-static loading (present paper); ii) fragmentation of impact-loaded quartz bars [18-20], iii) ZrO_2 [20-23] and SiC [21] ceramics fragmentation in a Hopkinson pressure bar test, iiiii) syminal (synthetic mineral alloy) fragmentation under high-speed impact [20]; iiiiii) fragmentation of tubular alumina (Al_2O_3) samples under shock-wave loading [24,25]. The main parameter, which governs fragmentation statistics, is the specific strain energy $E(J/kg)$. Due to the usage of different loading setups, it is impossible to evaluate specific energy using the same method. But the



fragmentation intensity can be characterized by the number of fragments per unit mass, N_m , which is easy to determine for all types of loads and which varies with the specific strain energy as the power law, Fig. 10.

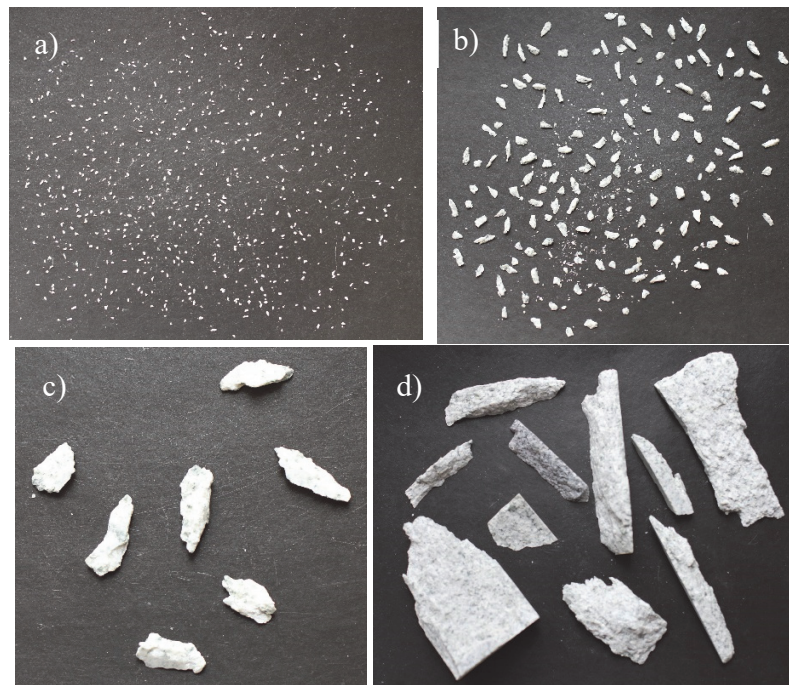


Figure 7: Fragments photo for sieve size: a) 0.63 mm; b) 3 mm; c) 7mm; d) more than 15 mm.

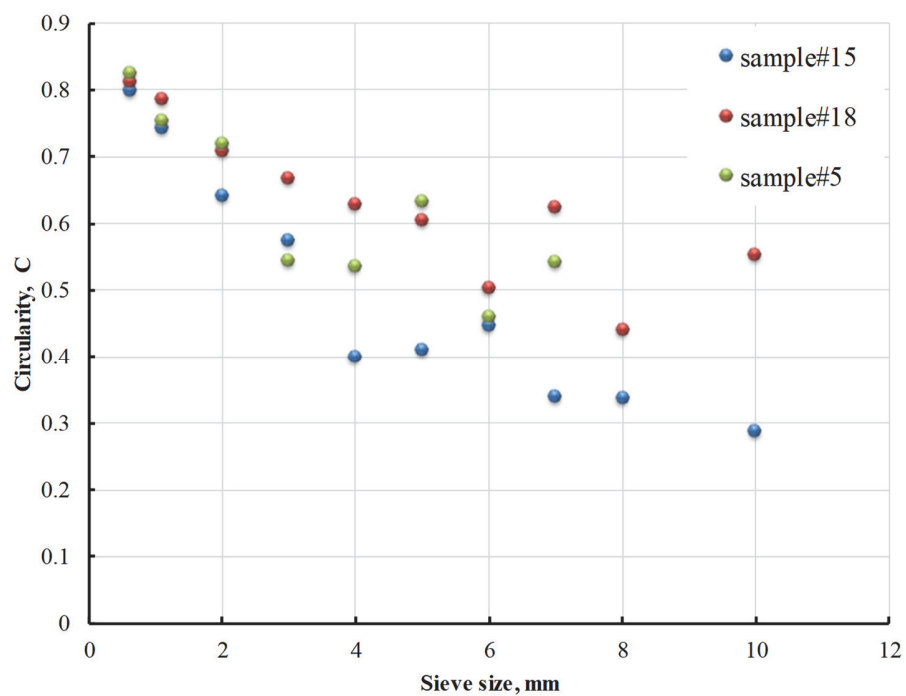


Figure 8: Circularity vs sieve size for three samples.

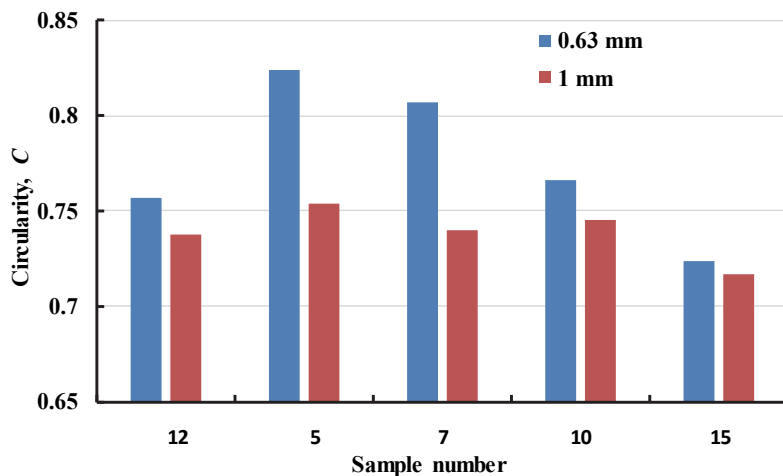


Figure 9: Circularity for five samples: blue indicates circularity for fragments in sieve with cell size 0.63 mm; red for cell size 1 mm.

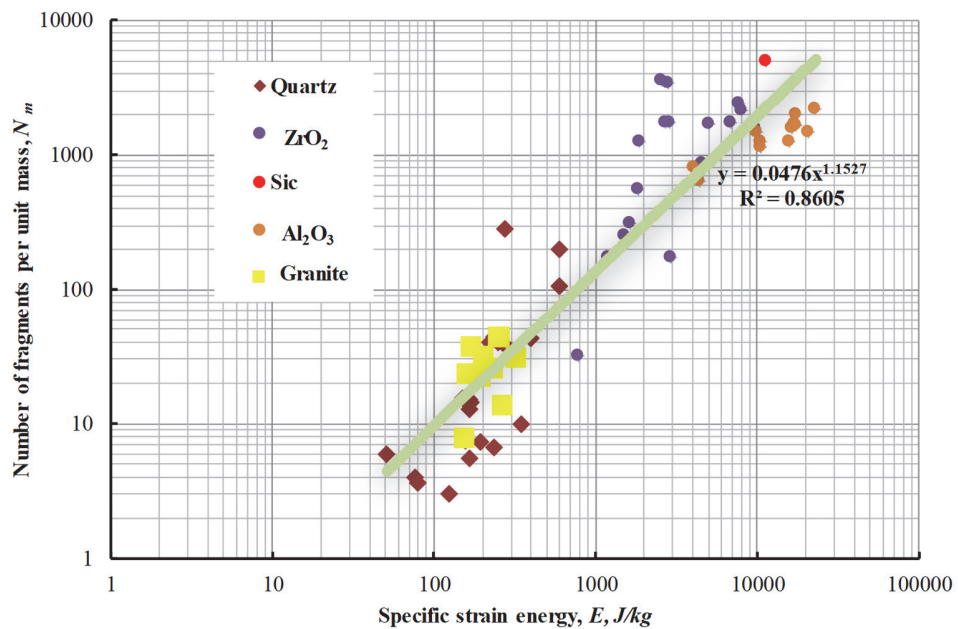


Figure 10: Fragment number per unit mass vs specific strain energy.

Dependence of power law exponent, D , from number of fragments per unit mass, N_m , has been analyzed for five materials (quartz, ZrO_2 and SiC ceramics, syminal and granite), which exhibits power law as fragment size distribution, Fig.11. Alumina fragment size distribution is the combination of power and exponential laws. The quantity D depends on the load intensity (specific strain energy E), material structure (the porosity of ZrO_2 ceramics samples varied from 2% to 30%), and specimen pre-treatment (end polishing, strict parallel alignment, flatness of contact with the bars). As is seen from Fig.11, preliminary treatment of ceramic specimens (data within an oval) significantly reduces the spread of the distribution exponent, D . Data analysis suggests that D increases with the rising number of fragments per unit mass (with the rising load intensity). To compare fragmentation process of granite, quartz and ceramic, we construct on the same plot fragment size distribution for three samples (Fig.12) with similar values of fractal dimension D (which characterizes fragmentation process): for granite $D=1.95$; for quartz $D=2.09$; for ZrO_2 $D=2.03$ (with porosity 30%). The samples are indicated by arrows on Fig. 11. The value, r , on the plot shown in Fig.12 is expressed as:

$$r = \sqrt[3]{\frac{m}{M_T}} \quad (4)$$



where m is the fragment mass, and M_T is total fragment mass.

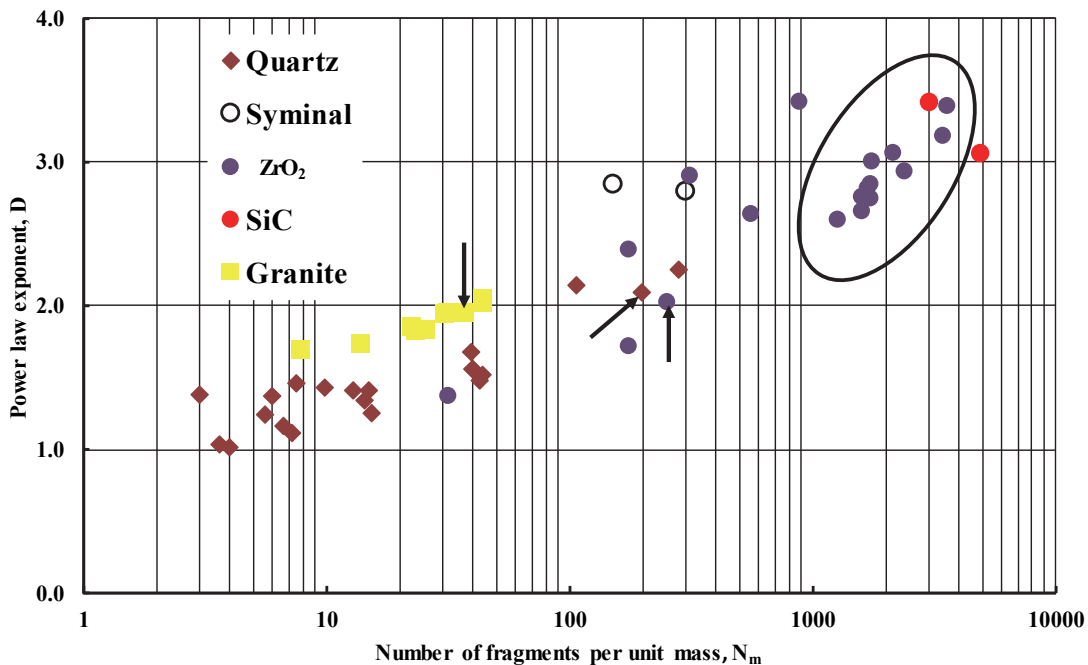


Figure 11: Power law exponent of fragment size distribution for five tested materials.

The analysis of Fig.10 and Fig.11 shows that we can get the similar distribution for granite, quartz and ceramics, but at different value N_m . In this case the relation for fragmentation intensity, N_m , is:

$$\text{granite } N_m < \text{quartz } N_m < \text{ceramic } ZrO_2 N_m \quad (5)$$

Inequality (5) describes the real resistance to fracture of these materials. For fragmentation of ZrO_2 ceramics (even with high porosity about 30%), we need to expend more energy than for fragmentation of quartz and granite.

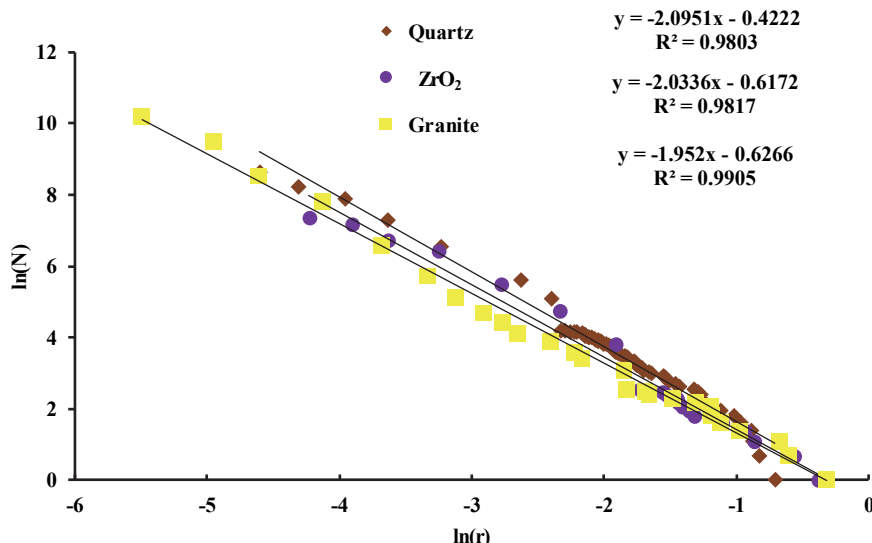


Figure 12: Fragment size distribution for 3 materials with power law exponents: for granite $D = 1.95$; for quartz $D = 2.09$; for ZrO_2 $D = 2.03$



CONCLUSION

Fragmentation of Mansurov granite under quasi-static loading described by power law (Fig.2(b)) in the range of fragment mass from 4.5×10^{-5} g to 500 g (7 orders). The shape of the fragments changes from splinter (circularity 0.3) to oval (circularity 0.8). The increasing in the circularity and the number of grains with the size equal to about 1mm explains the sharp growth of the fragments number with the size about 1mm. This fact can be caused by chipping of feldspar grains. Thus, it can be concluded that along with the cracking for the formation of small fragments, we have an additional failure mechanism, which is caused by grain disintegration.

ACKNOWLEDGMENT

We thank our colleagues from Nano-mineralogy Sector of Perm State University who provided the structure study of granite.

This work is supported by Russian Foundation for Basic Research, grant 16-41-590-779-p_a.

REFERENCES

- [1] Turcotte, D. L., *Fractals and Chaos in Geology and Geophysics*, second ed., Cambridge University Press, (1997).
- [2] Grady, D.E., Lipkin, J., Criteria for impulsive rock fracture, *Geophysical Research Letter*, 7(1980) 255-258. DOI: 10.1029/GL007i004p00255.
- [3] Grady, D.E., Kipp, M.E., Dynamic rock fragmentation, in: B.K. Atkinson (Eds.), *Fracture mechanics of rock*, Academic Press, London, (1987) 429-475.
- [4] Bowman, E. T., Dynamic rock fragmentation: thresholds for long runout rock avalanches, *Frattura ed Integrità Strutturale*, 30 (2014) 7-13. DOI: 10.3221/IGF-ESIS.30.02.
- [5] Wang, S.R., Li, C.Y., Zou, Z.S., Liu, X.L., Acoustic emission characteristics of instability process of a rock plate under concentrated loading. *Avalanches, Frattura ed Integrità Strutturale*, 36 (2016) 182-190. DOI: 10.3221/IGF-ESIS.36.
- [6] Panteleev, I., Plekhov, O., Pankov, I., Evseev, A., Naimark, O., Asanov, V., Experimental investigation of the spatio-temporal localization of deformation and damage in sylvite specimens under uniaxial tension, *Engineering Fracture Mechanics*, 129 (2014) 38-44. DOI:10.1016/j.engfracmech.2014.08.004.
- [7] Vettegren, V.I., Kuksenko, V.S., Shcherbakov, I.P., Dynamics of microcracks and time dependences of surface deformation of a heterogeneous body (granite) under an impact. *Physics of the Solid State*, 54(7) (2012) 1425-1429. DOI:10.1134/S1063783412070347.
- [8] Chmel, A., Sherbakov, I., Damage initiation in brittle and ductile materials as revealed from a fractoluminescence study, *Frattura ed Integrità Strutturale*, 30 (2014) 162-166. DOI: 10.3221/IGF-ESIS.30.21.
- [9] Kawaguchi, Yo., Charged particle emission and luminescence upon bending fracture of granite, *Japanese Journal of Applied Physics*, 37(6A) (1998) 3495-3499. DOI: <https://doi.org/10.1143/JJAP.37.3495>.
- [10] Panteleev, I., Mubassarova, V., Damaskinskaya, E., Naimark, O., Bogomolov, L., Influence of weak electric field on spatialoral dynamics of damage evolution during granite deformation. *AIP Conference Proceedings*, 1683 (2015) 020177, DOI: <http://dx.doi.org/10.1063/1.4932867>.
- [11] Chen, Yo., Nishiyama, T., Ito, T., Application of image analysis to observe microstructure in sandstone and granite, *Resource geology*, 51(3) (2001) 249-258. DOI: 10.1111/j.1751-3928.2001.tb00096.x.
- [12] Kurlenya, M.V., Yakovitskaya, G.E., Kulakov, G.I., Stages in the fracturing process based on EME studies, *Journal of Mining Science*, 27(1) (1991) 39-43. DOI:10.1007/BF02499684.
- [13] Kurlenya, M.V., Kulakov, G.I., Yakovitskaya, G.E., Spectral-time analysis of electromagnetic emission during crack formation in ore specimens, *Journal of Mining Science*, 29(1) (1993) 3 -13. DOI:10.1007/BF00734323.
- [14] Kulakov, G.I., Yakovitskaya, G.E., Method of predicting the fracture of rocks using the features of the spectral-time characteristics of signals of electromagnetic radiation, *Journal of Applied Mechanics and Technical Physics*, 36(6) (1995) 928-932. DOI:10.1007/BF02369392.



- [15] Vostretsov, A.G., Kulakov, G.I., Timonenkov, Yu.A., Yakovitskaya, G.E., Prediction of rock failure from spectral characteristics of signals from electromagnetic radiation, Journal of Mining Science, 34(4) 1998 296-299. DOI: 10.1007/BF02803688.
- [16] Carpinteri, A., Chiodoni, A., Manuello, A., Sandrone, R. Compositional and microchemical evidence of piezonuclear fission reactions in rock specimens subjected to compression tests, Strain, 47 (2011) 282–292. DOI: 10.1111/j.1475-1305.2010.00767.x.
- [17] Carpinteri, A., Cardone, F., Lacidogna, G. Energy Emissions from Failure Phenomena: Mechanical, Electromagnetic, Nuclear, Experimental Mechanics, 50 (2010) 1235–1243. DOI:10.1007/s11340-009-9325-7.
- [18] Davydova, M., Uvarov, S., Fractal Statistics of Brittle Fragmentation. Frattura ed Integrità Strutturale, 24 (2013) 60-68. DOI: 10.3221/IGF-ESIS.24.05.
- [19] Davydova, M.M., Uvarov, S.V., Naimark, O.B., Scale invariance in dynamic fragmentation of quartz, Physical Mesomechanics, 17(1) (2014) 81–88. DOI: 10.1134/S1029959914010093.
- [20] Davydova, M., Uvarov, S., Chudinov, V., Scaling law of quasi brittle fragmentation, Procedia Materials Science, 3 (2014) 580-585. DOI: 10.1016/j.mspro.2014.06.096.
- [21] Davydova, M., Uvarov, S., Chudinov, V., Statistical laws of dynamic fragmentation of ZrO_2 ceramics, Applied Mechanics and Materials, 784 (2015) 468-475. DOI:10.4028/www.scientific.net/AMM.784.468.
- [22] Davydova, M., Uvarov, S., Scaling laws of structure and fragmentation parameters of ZrO_2 ceramics, Procedia Structural Integrity, 2 (2016) 1936–1943. DOI:10.1016/j.prostr.2016.06.243.
- [23] Davydova, M.M., Uvarov, S.V., Naimark, O.B., Space-time scale invariance in dynamically fragmented quasi-brittle materials, Physical Mesomechanics, 19(1) (2016) 86–92. DOI: 10.1134/S1029959916010094.
- [24] Bannikova, I.A., Uvarov, S.V., Naimark, O.B., Analysis of fragmentation statistics of alumina tubular specimens, AIP Conference Proceedings, 1623 (2014) 59–62. DOI: 10.1063/1.4898882.
- [25] Bannikova, I.A., Naimark, O.B., Uvarov, S.V. Transition from multi-center fracture to fragmentation statistics under intensive loading, Procedia Structural Integrity, 2 (2016) 1944–1950. DOI: 10.1016/j.prostr.2016.06.244.